

Optomechanics of Chiral Dielectric Metasurfaces

Simone Zanotto,* Alessandro Tredicucci, Daniel Navarro-Urrios, Marco Cecchini, Giorgio Biasiol, Davide Mencarelli, Luca Pierantoni, and Alessandro Pitanti

The coupling between electromagnetic fields and mechanical motion in micro- and nanostructured materials has recently produced intriguing fundamental physics, such as the observation of mesoscopic optomechanical phenomena in objects operating in the quantum regime. It is also yielding innovative device applications, for instance in the manipulation of the optical response of photonic elements. Following this concept, here it is shown that combining a nanostructured chiral metasurface with a semiconductor suspended micromembrane can open new scenarios where the mechanical motion affects the polarization state of a light beam, and vice versa. Optical characterization of the fabricated samples, assisted by theory and numerical modeling, reveals that the interaction is mediated via moving-boundary and thermoelastic effects, triggered by intracavity photons. This work represents a first example of “Polarization Optomechanics,” which can give access to new forms of polarization nonlinearities and control. It can also lead to wide applications in fast polarimetric devices, polarization modulators, and dynamically tunable chiral state generators and detectors.

Rapid technological advancements in micro- and nano-fabrication have recently led to a class of photonic resonators strongly intertwined with mechanical elements.^[1] This opened the way to a new field—Cavity Optomechanics—enabling photonic solid-state devices that show exceptional properties: as an example, one could cite the ground state cooling of motional modes in a mesoscopic system through radiation pressure.^[2] A proper assessment of the mechanical motion in optomechanical systems can further be used to strongly influence the output light, not only at a quantum level, producing squeezing^[3,4] and nonclassical states.^[5] but even in a classic picture, with chaotic light^[6] and low-power, fast intensity modulation.^[7–9]

On the other side, nanoscale artificial materials have been the major object of research in the field of electromagnetic structured media for more than two decades.^[10–15] Wavelength-scale patterns

of scatterers have shown the capability to produce bright colors and extravagant surface effects, often mocking what elegantly realized in biological systems.^[16] In particular, nanostructuring techniques, combined with powerful *ab initio* design tools, allow to develop materials which show a chiral response far larger than their natural counterparts, i.e., stereochemical compounds.^[17–22]

In this article, we report how an all-dielectric chiral metasurface, defined on a mechanically compliant GaAs membrane, can couple its fundamental mode of vibration to the light polarization state—noticeably, imprinting its chiral content. Conversely, the polarization state of the photons addressing the device can deeply influence the mechanical resonator by shifting its resonance frequency through an optothermal spring effect. Mechanical elements have been previously conjoined with optical metamaterials to augment the functionalities provided by the bare photonic patterning;^[23–35] however, fast light polarization and chirality manipulation has never been addressed so far. In addition, previous reports of mechanically reconfigurable metasurfaces were based on metallic scatterers, which offer limited performances due to ohmic losses; on the contrary, in the all-dielectric system we are relying on, optical losses are extremely weak, allowing for sharp and definite resonances originating from the high refractive index contrast between the patterned semiconductor and the surrounding (air or vacuum). The large oscillation frequency, exceeding 300 kHz, makes this new kind of device appealing for possible future fast polarization modulators or polarimeters, but the concept could


Dr. S. Zanotto, Prof. A. Tredicucci, Dr. M. Cecchini, Dr. A. Pitanti
Laboratorio NEST – Scuola Normale Superiore, and Istituto
Nanoscienze – CNR
Piazza San Silvestro 12, 56127 Pisa, Italy
E-mail: simone.zanotto@nano.cnr.it

Prof. A. Tredicucci
Dipartimento di Fisica
Università di Pisa
Largo B. Pontecorvo 3, 56127 Pisa, Italy

Dr. D. Navarro-Urrios
MIND-IN2UB
Departament d'Enginyeria Electrònica i Biomèdica
Facultat de Física
Universitat de Barcelona
Martí i Franquès 1, 08028 Barcelona, Spain

Dr. G. Biasiol
Istituto Officina dei Materiali CNR
Laboratorio TASC
34149 Basovizza (TS), Italy

Dr. D. Mencarelli, Prof. L. Pierantoni
Università Politecnica delle Marche
60131 Ancona, Italy

 The ORCID identification number(s) for the author(s) of this article can be found under <https://doi.org/10.1002/adom.201901507>.

© 2019 The Authors. Published by WILEY-VCH Verlag GmbH & Co. KGaA, Weinheim. This is an open access article under the terms of the Creative Commons Attribution-NonCommercial License, which permits use, distribution and reproduction in any medium, provided the original work is properly cited and is not used for commercial purposes.

DOI: 10.1002/adom.201901507

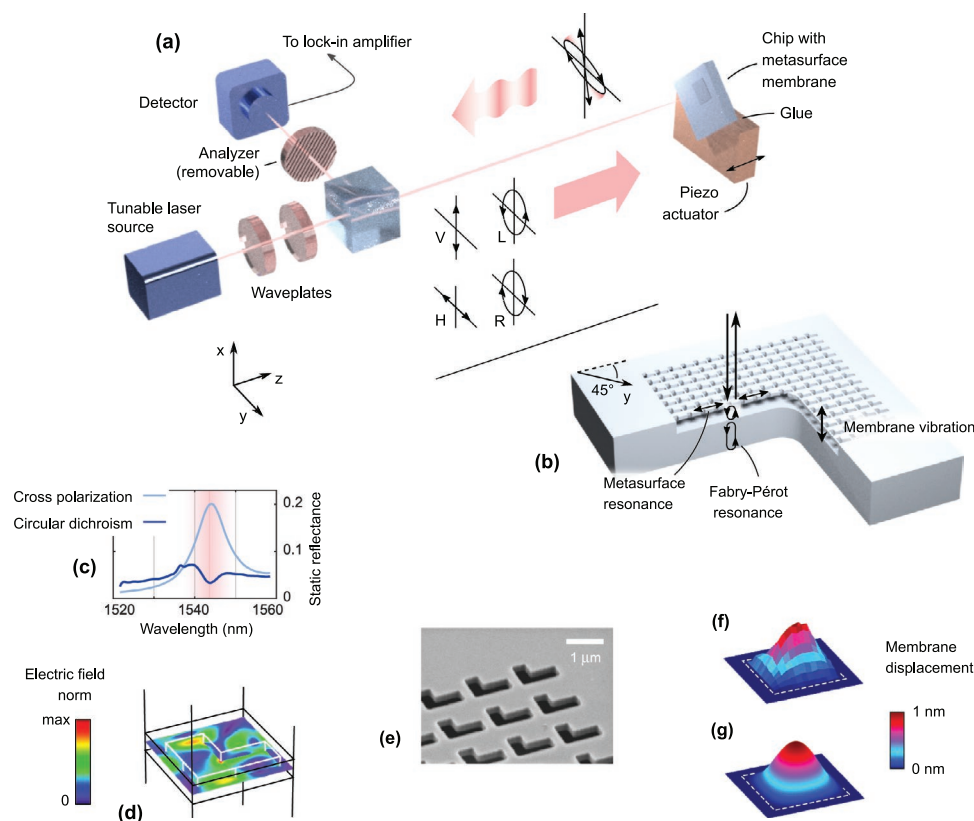


Figure 1. Optomechanics of a chiral metasurface. a) Sketch of the setup employed in the experiment and schematics of the effects observed. A laser beam with controlled polarization is reflected off the metasurface, with its intensity and polarization modulated in time. The chip with the metasurface membrane can be mounted in a vacuum chamber (not shown) to enhance the mechanical resonance quality factor. The chip is represented, with a cross-cut, in (b). It consists of a semiconductor (GaAs) membrane patterned with L-shaped holes, responsible for a chiral resonance arising from the combined metasurface and Fabry–Pérot effects. Further details of the metasurface (hole sizes, thicknesses, etc.) are reported in the Supporting Information. The photonic response is sensitive to the membrane vibration, as it affects the Fabry–Pérot length. c) Chiro-optical effects occur in the wavelength range relevant for telecommunications. Here, the Fabry–Pérot effect is filtered out and the cross-polarized (H-polarized input, V-analyzed output) and circular dichroism (difference between reflection spectra with right/left circularly polarized inputs) curves are fingerprints of the metasurface resonance only. The field profile of the mode responsible for such effects is plotted in (d), where one unit cell of the metasurface is represented. e) Scanning electron micrograph of the metasurface. f,g) Illustration of the membrane displacement occurring when the fundamental mode is excited, respectively, in an experiment (laser Doppler vibrometry) and in a finite-element model.

potentially be even more interesting at the quantum level, as optomechanical coupler for polarization-encoded photon states.

Our device consists of a gallium arsenide (GaAs) square membrane patterned with L-shaped holes, lying at micrometer-scale distance from a flat-interface substrate (Figure 1). Membrane-based metasurface optomechanical devices have been the object of some previous investigations, however, with different goals with respect to ours: for instance, in ref. [34], the main purpose was that of controlling mechanical damping with light, while in refs. [26,27] the focus was on reflection and absorption tuning. The main peculiarity of our device resides instead in the use of a chiral pattern, with the consequent possibility to enable polarization-dependent optomechanical effects; moreover, as highlighted above, the choice of a dielectric material (GaAs) allows for almost lossless operation. GaAs has also other advantages: it is easily machinable,^[36] it can host active elements,^[37–39] and it has strong nonlinear optical response.^[13,40–43] Furthermore, being its refractive index similar to that of silicon, the design presented here can be straightforwardly exported to complementary

metal-oxide-semiconductor (CMOS)-compatible platforms for eventual integrability with electronics. Few GaAs-based optomechanical devices have also been reported,^[9,44,45] none of them, however, including chiral metasurfaces.

The chosen “L-shaped” pattern design is a minimal one (see the scanning electron microscope micrograph of Figure 1e); this is the simplest shape that breaks in-plane mirror symmetry, granting for 2D-chirality. When the patterned membrane is considered in conjunction with the underneath substrate, the overall structure becomes truly 3D-chiral. Details on the fabrication process can be found in the Experimental Section. The photonic response of the structure is thus a combination of two effects: the resonance of the sole patterned membrane^[46] and the multiple Fabry–Pérot resonances determined by membrane–substrate optical paths, as sketched in Figure 1b. Due to interference, the overall device optical response depends on the relative membrane to substrate distance; this gives rise to a form of optomechanical coupling which we exploit in our experiment. The membrane vibration impacts on the phase, intensity, and polarization of light and therefore can be investigated

by looking at the device optical response. This is done using a standard free space setup where the polarization state of input light can be easily controlled, as shown in Figure 1a. In our experiment, membrane oscillations are forced by a piezoelectric actuator, and the coherent response is detected through a lock-in amplifier (see the Experimental Section). The mechanical mode we use is the fundamental one (Figure 1f). The simulated mode profile (with resonance predicted to occur at 0.34 MHz, Figure 1g) well reproduces the displacement field evaluated in the interferometric measurement.

The mechanical effect on the optical response of the device can be described by means of reflection matrices, which describe the amplitude, phase, and polarization response of the metasurface–substrate complex. The reflection matrix R connects the incident and the reflected wave field components by $\mathbf{E}_r = R \mathbf{E}_i$, where $\mathbf{E}_{i,r} = (E_{i,r,x}, E_{i,r,y})$ are the Cartesian components of the complex electric field vector associated with the propagating waves. In addition to the fixed metasurface geometric parameters, the R matrix depends on the metasurface–substrate distance ζ ; we assume that the focused laser beam, smaller than the membrane size, locally probes rigid membrane shifts, leading to approximating ζ as a constant number, independent of the position across the membrane. We can hence write, for small oscillation amplitudes

$$R = R(\zeta) = R_0 + R_1 \Delta\zeta \quad (1)$$

where $R_1 = \partial R / \partial \zeta$, and $\Delta\zeta$ is the displacement from the rest position. From this, the static and dynamic response of the metasurface can be easily determined.

The static response is encoded in R_0 . As an example, experimental cross-polarized (horizontally polarized input, vertically analyzed output) and circular dichroism (CD; difference between

output intensities for right-circular and left-circular inputs) reflection spectra are reported in Figure 1c, where the Fabry–Pérot oscillations have been removed by means of a smoothing procedure for the sake of clarity; the original spectra are reported in the Supporting Information. Our formalism well reproduces the measured spectra which mainly consist of a broad resonant feature centered at about 1545 nm. The simulated field profile of the corresponding optical mode is reported in Figure 1d.

The dynamical response consists of a modulation of phase, amplitude, and polarization state of the reflected wave (R_1) around the point dictated by the static response (R_0). Particular forms of static and dynamic reflectivities can be targeted at the design stage; in particular, it has been theoretically predicted that, using an appropriate complex metasurface unit cell, arbitrary control on the reflectivities can be achieved.^[47,48] On the other hand, our device employs a minimal design, resulting from the maximization of CD at 1550 nm. Despite its simplicity, it offers a rich landscape of static responses in its spectrum of operation (i.e., both positive and negative circular and linear dichroisms) and perfectly illustrates the physics behind static and dynamic control of polarization states. This is shown by performing a modulation experiment where the incident polarization is kept fixed to the horizontal (H) state (Figure 2), and the intensity modulation of the reflected wave is detected. To fully illustrate the metasurface dynamical response, we devised two measurements, with and without a linear polarizer placed in the reflected beam with vertical (V) pass axis. The results are reported in Figure 2b, together with the simulations for comparison; the theoretical formalism is provided in the Supporting Information. Note that the modulation spectrum shows evident fringes, dictated by multiple Fabry–Pérot resonances; superimposed to it a weak envelope centered around the metasurface resonance can be observed. The measurement

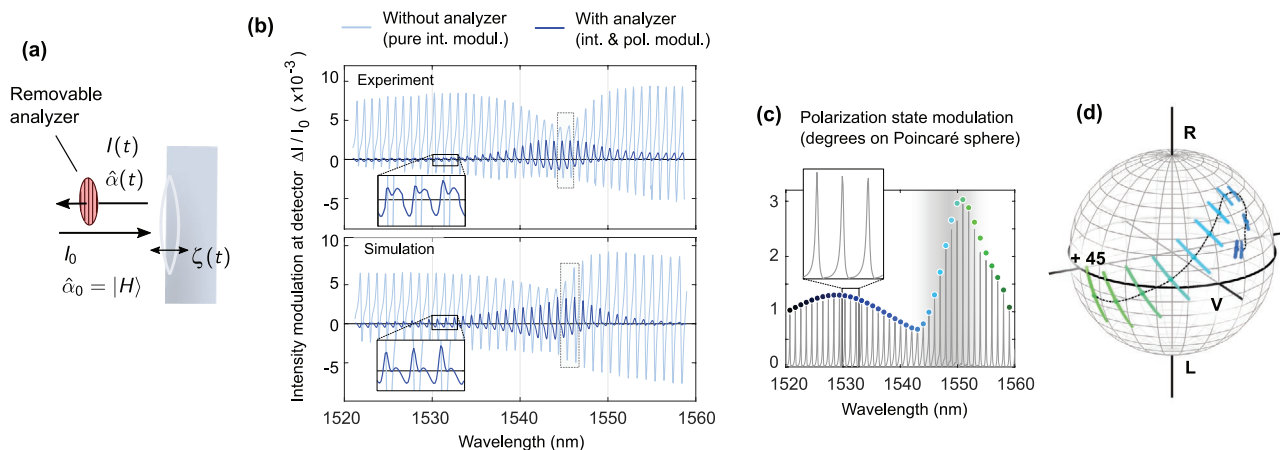


Figure 2. Optomechanical fingerprints on linear polarization. a) Schematic of the experiment. Linearly horizontally polarized light (see also Figure 1 for the convention) is incident with a constant intensity on the metasurface. As the membrane oscillates in time (0.8 nm oscillation amplitude), intensity and polarization are modulated, as reported in (b). The traces show the wavelength-dependent intensity modulation observed at the detector, i.e., after the sample and a possible linear analyzer. Light blue traces are obtained without the analyzer, hence quantifying the pure intensity modulation. Dark blue traces are obtained with the analyzer, thus containing contributions from both intensity and polarization modulation. The wavelength range highlighted in the gray box is the object of further analysis (see Figure 4). The fast wavelength oscillations are due to the Fabry–Pérot effect in the substrate. c) Calculated polarization modulation spectrum for the same experimental conditions. d) Polarization rotation and modulation represented on the Poincaré sphere around the metasurface resonance (each colored segment corresponds to the wavelength of a peak of the curve in (c), in the gray-shaded region). The center of each segment is the steady-state output polarization, still for H-polarized input. Oscillation amplitude is here assumed to be 3 nm.

without the analyzer indicates that the metasurface oscillation is capable of inducing an intensity modulation by acting on the modulus of the reflected field $|E_r|^2$; by comparing this spectrum with what obtained with the analyzer, an interesting feature appears: the cross-polarized spectrum (dark blue curve) shows a completely different wavelength dependence, evidencing a dynamic polarization state modulation. If the polarization state were only rotated in a static way, the cross-polarized modulation spectrum would be simply a fraction of the spectrum taken without analyzer; as this is not the case, it means that the *polarization state itself* is modified by the mechanical motion.

To better clarify this aspect, we performed further theoretical analysis in the direction of full dynamic polarimetry of the reflected light. Having access to the matrices R_0 and R_1 , it is straightforward to determine the Stokes parameters of the reflected radiation and its dependence on the displacement $\Delta\zeta$. A natural metric to quantify the polarization modulation effect is to measure the distance between two points on the Poincaré sphere calculated for $\Delta\zeta = 0$ and $\Delta\zeta = 0.8$ nm (i.e., the membrane displacement measured in the experiment discussed above). This distance, stated in terms of the angle subtended between the two polarization points and the sphere center, is plotted with its spectral dependence in Figure 2c, where we highlighted the peak maxima with circular markers. Both the strong Fabry–Pérot oscillations and the envelope effect of the metasurface resonance are still evident. A maximum polarization state modulation of roughly 0.02 rad nm^{-1} can be appreciated. By increasing the piezoelectric actuator driving voltage, we can linearly increase the harmonic modulation value up to about 0.2 rad (when the device operates in vacuum). The system main limitation occurs when the mechanical motion becomes nonlinear, giving rise to an anharmonic time dependence, which in any case can still produce modulation amplitude exceeding 0.5 rad (see the Supporting Information).

More insights are gained by looking at the actual location of the polarization state on the Poincaré sphere and at the path followed by the polarization point on the sphere when mechanical oscillation occurs. These important features are illustrated in Figure 2d. Here, we analyzed a selection of wavelengths close to the metasurface resonance (peaks of Figure 2c in the gray-shaded area). The colored segments on the sphere represent the polarization modulation occurring when $\Delta\zeta$ is tuned from -3 to 3 nm. Such a larger displacement is still experimentally accessible, as discussed, at the expense of losing perfect mechanical linearity. When the modulation is mapped on the Poincaré sphere (Figure 2d), it illustrates a very interesting behavior: in the metasurface resonance region, *both* static polarization state *and* polarization modulation “direction” can be chosen in a nontrivial way. Here, the tuning parameter is wavelength; more generally, static and dynamic polarization response can be chosen by appropriately targeting wavelength and geometric parameters. It can be envisaged that more complex structures, which go beyond the proof-of-principle L-shaped array analyzed here, could lead to designer’s targeted polarization and wavelength response.

Linear polarization rotation is a precursor of chirality, in the sense that chiral objects generally rotate the polarization plane of a linearly polarized beam. However, a more

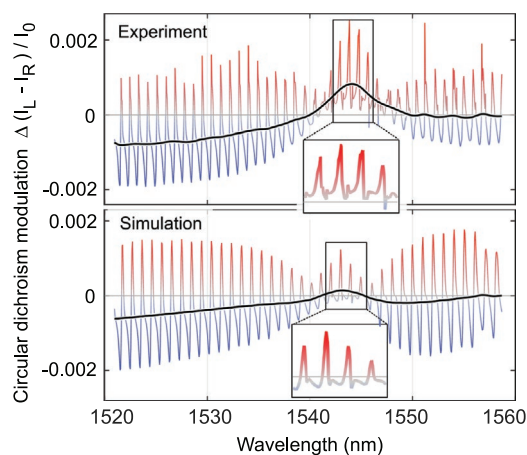


Figure 3. CD modulation occurring upon mechanical oscillation of the membrane. Narrow wavelength features are due to Fabry–Pérot interference occurring in the substrate, while the envelope shape is dictated by the metasurface resonance.

direct measure of electromagnetic chirality is CD. We hence measured the optomechanical effect on CD by measuring its modulation induced by membrane oscillation. The result is illustrated in **Figure 3**: the spectral behavior displays clear fingerprints well reproduced by the full wave electromagnetic simulation, even in their finer details. These data witness two main points. First, the device is a wavelength-sensitive modulator acting on circular polarization, which can replace other technologies like liquid crystal-based modulators. The advantage lies in the possibility to avoid any encapsulation technique needed to confine the liquid phase, which hinders miniaturization and integration of the components; moreover, the actuation frequency of our device is larger than that typically achieved in liquid crystal devices (hundreds of kHz, potentially MHz, vs tens of kHz). Also, despite the narrow operation bandwidth of our prototype, improved designs can be conceived to target specific operation wavelengths and modulation frequencies. Second, mechanical oscillations act on the proper, near-field-based electromagnetic chirality of the metasurface, eventually connected to the capability that local fields have to excite chiral molecules.^[49–51] Since this mechanism can be employed to discriminate between the helicity of analytes, our chirality tuning method may be employed in sensing platforms where the local electromagnetic chirality is required to be modulated at a high frequency.

The phenomena analyzed so far have been studied in ambient conditions. While this demonstrates the robustness of the sample, the presence of air at atmospheric pressure degrades the mechanical quality factor, preventing a full exploitation of the potential of the optomechanical interaction. To this end, we enclosed the sample in a vacuum chamber and analyzed again the mechanical response.

At first, we focused on the light response to a linearly H-polarized input. The detected signal (amplitude channel of the lock-in) is reported in **Figure 4a**, as a function of laser wavelength and mechanical driving frequency. In the analyzed range, which spans slightly more than one Fabry–Pérot fringe,

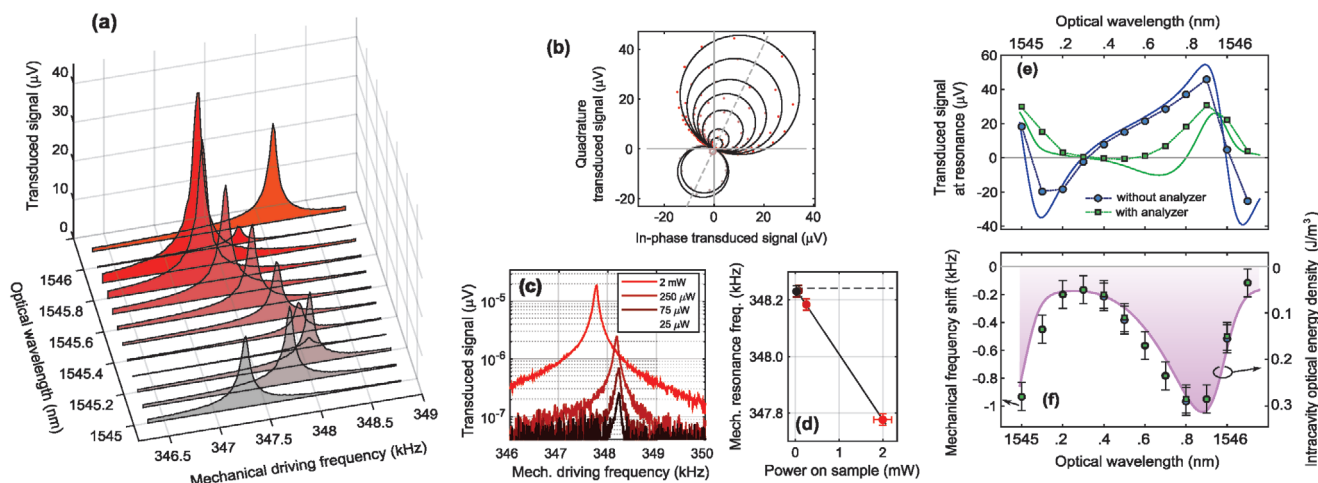


Figure 4. Optomechanical spring effect in the high mechanical Q-factor regime. a) Evolution of the mechanical resonance, in vacuum around one Fabry–Pérot fringe, with both peak value and central frequency depending on the optical wavelength; input polarization is H and no analyzer is present. b) Fit of the transduced signal in the in-phase/quadrature space. c) Dependence of the transduced mechanical spectrum upon optical power and d) resonance red-shift with optical power. e) Optical wavelength dependence of the transduced signal peak value across one Fabry–Pérot fringe (region in the gray-shaded area of Figure 2b). Both measurements with and without an output analyzer (solid symbols) are well reproduced by simulations (solid lines). f) Wavelength dependence of the spring effect. No dependence on the output polarization filtering is observed, and the data are strictly correlated with the intracavity energy density.

different levels of modulation amplitude can be observed, as well as different amounts of redshift in the mechanical resonant frequency. The last effect is now visible since the air-induced damping is almost completely eliminated: at the base pressure of 3×10^{-5} mbar, the mechanical features can be well fitted with Lorentzian lineshapes holding linewidths as narrow as 0.15 kHz, translating in mechanical Q-factors of about 2000. Further insights into the mechanical resonance response can be obtained by looking at the in-phase/quadrature space data (i.e., X vs Y lock-in channel data) that are reported in Figure 4b. Here, for each laser wavelength, the transduced signal data form a circle: this feature is the counterpart of the observation of a Lorentzian in the amplitude channel, and testify that the membrane resonance complies with a linear oscillator model. The data of Figure 4a,b have been obtained with an excitation voltage of $300 \mu\text{V}_p$ and laser power of 2 mW.

The mechanical frequency shift depends on the optical power; such a dependence is linear as shown in Figure 4c,d (data collected for laser wavelength = 1545.5 nm). Figure 4e shows how the transduced amplitude signal at the mechanical resonance peak varies with the optical wavelength. Here, the experiment has been run both in absence and in presence of the analyzer (see Figure 2a); similarly to what already observed in Figure 2b, the very different spectral shapes of the transduced signal with and without the vertical analyzer confirm the fact that the device has modulating intensity and polarization in a nontrivial way. Note that the simulations (solid lines, scaled on the y-axis by the same, arbitrary value) well reproduce the experimental results (dot-connected full markers). More interestingly, the two-axis plot of Figure 4f shows that the spectral shift of the mechanical resonator is strongly correlated with the intracavity photon energy density. This effect has a genuine optomechanical nature and can be understood as an optical spring effect: the presence of the electromagnetic field in the structured metasurface modifies the effective Hooke

constant of the equivalent mass-spring system. To understand the origin of this effect in our device, it is necessary to go beyond the coupled-mode analytical model well known in the optomechanics community.^[1,52] Numerical analysis (see Supporting Information, Sections S3.5–S3.6) supports the vision that a form of direct optothermal spring effect is leading the optomechanical response. Key feature of this kind of coupling is the linear relation $\Omega = \Omega_0 + k_{OT} w_{cav}$, where Ω is the membrane mechanical resonance frequency, w_{cav} is the intracavity electromagnetic energy density and $k_{OT} \cong -2.1 \times 10^4 \text{ Hz m}^3 \text{ J}^{-1}$ is the optothermal constant. In this model, the mechanical frequency shift $\Omega - \Omega_0$ has always the same sign (negative), and it is linearly dependent on the incident intensity. Furthermore, no major effects on the mechanical linewidth are expected. In the studied device, the effects of the radiation pressure force are ruled out, as they change sign in the relevant wavelength range and because they are far too small to justify the observed shifts (see Supporting Information, Section S3.6). Electrostriction effects can also be safely neglected even assuming the large photoelastic coefficients of GaAs.^[53] In other words, a little residual absorption, likely attributable to impurities in the semiconductor, drives a wavelength-dependent heating of the metasurface, with a consequent relaxation of its effective spring constant. The upper bound for temperature rise is estimated to be a fraction of Kelvin, as detailed in the Supporting Information. We highlight that the residual optical absorption does not prevent our dielectric metasurface to definitely outperform the metal-based counterparts: while in the latter absorbance values of 10% are commonly encountered, our device features values of the order of 0.1%.

The optical spring effect is one of the cornerstones of cavity optomechanics, and one of the main signs of back-action effects; as such it has been observed in several systems.^[1] Nonetheless, the interplay between this effect and light polarization has been explored far less; to date, only few theoretical studies

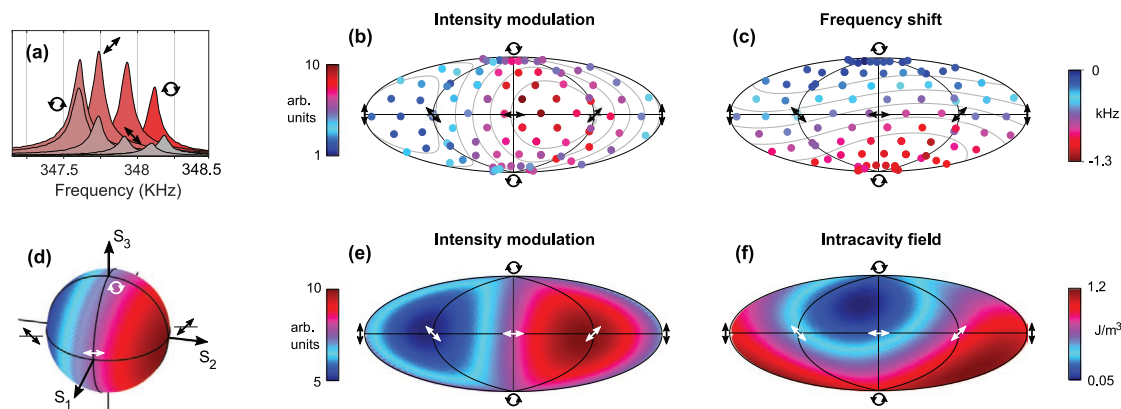


Figure 5. Observation of chiral spring effect. a) Mechanical resonance evolution as a function of the chirality of input light. Full polarimetric analysis of modulation amplitude and frequency shift b,c) shows a different mapping on the projected Poincaré sphere. Continuous lines are spherical harmonics. d–f) The experimental results are validated by the simulations. While (e,f) are plotted in the same configuration as the experimental data, panel (d) offers a different, 3D representation of the results of panel (e). The frequency shift is negatively correlated with the intracavity energy density, confirming the thermal nature of the chiral spring effect.

can be found on the topic.^[31] Our device has proven instead to be a precious test-bed for understanding how the optical forces can be harnessed by means of polarization; moreover, it revealed an intriguing interplay between polarization-dependent optical forces and polarization-dependent optomechanical transduction. The experimental framework is the same as previously described, with the difference that here light wavelength is kept fixed at 1545.8 nm and that the polarization state of the probe beam is continuously tuned across the Poincaré sphere. The results are reported in **Figure 5**. Panel (a) illustrates that the mechanical transduction curve changes resonance frequency and magnitude as a function of the light polarization state. In particular, the two opposite circular polarization states correspond to extreme values of the frequency shift, while the opposite diagonal linear polarization states correspond to extreme levels of optomechanical transduction. Note that here the transduced signal is entirely given by intensity modulation, as no analyzer is placed after the sample. In panel (b), we report the full polarimetric characterization of intensity modulation: each dot corresponds to an input polarization state set in the experimental process, while the gray lines are the level curves of zero and first-order spherical harmonics (more on this later). By comparison, panel (e) illustrates what is expected from the fully vectorial electromagnetic model (panel (d) provides an alternative representation on the 3D Poincaré sphere). As can be seen, we obtain a good agreement between experiment and simulations. Considering now the spring effect, panel (c) presents the mechanical frequency shift on the full polarization space. As previously observed, the shift (changed in sign) is correlated with the intracavity field (panel (f)), corroborating the picture that the spring effect has an optothermal origin. An additional feature of both optomechanical transduction and frequency shift is that they have a dipole-like dependence on the sphere. In other words, the quantities $\Delta I/I_0$ and $\Omega - \Omega_0$ have contributions from the zero and the first-order spherical harmonics, as expected from functions that are bilinear in the polarization Jones vector (see the Supporting Information). We finally notice that the intensity modulation and the frequency shift have a different—and almost

complementary—dependence on the polarization state; as an example, comparing the two polarimetric maps of Figure 5, we have almost zero CD modulation (the intensity modulation at the R and L poles are roughly the same), accompanied by a strong dependence of the frequency shift from the chirality of light (zero at the R pole, maximum at the L pole). While a specific reason for this behavior has not emerged, it clearly results from phenomenological observations supported by numerical data that in principle the observed optomechanical chiral effects can be exploited to implement a polarimeter based on a completely different mechanism with respect to ordinarily employed devices, having however the potential to be orders of magnitude faster.

In conclusion, we have demonstrated the coupling between nanoscale mechanical motion and optical chirality in a structured semiconductor membrane. This interaction manifests itself in two effects: from one side, fast linear and circular polarization modulation is realized; from the other, the mechanical resonant features are affected by the chirality of incident photons. With the potential to be scaled up to high-frequency mechanical mode (\approx GHz) coherently excited by surface acoustic waves, and thanks to the extreme design flexibility of artificially structured metamaterials, our device concept should strongly impact the field of polarization control. Furthermore, the polarization nonlinearity induced by the mechanical interaction can pave the way to complex and fast operations on the polarization state of light, like polarization squeezing. Given the ubiquity of polarized light in fundamental science and in applications, we believe that our proof-of-principle study will open new avenues in several fields such as biophotonics, material science, drug discovery, and telecommunications.

Experimental Section

The sample was fabricated by means of ordinary nanofabrication techniques (lithography, etching). Optomechanical characterization exploited the light of a tunable laser source, a mildly focusing polarization-resolved reflection setup, and a detector connected to

a lock-in amplifier. Independent characterization of the membrane vibration was done through a Laser Doppler Vibrometer. Numerical analysis was performed through rigorous coupled-wave analysis (MATLAB-based software PPML) and finite element method (COMSOL). Further details are given in the Supporting Information.

Supporting Information

Supporting Information is available from the Wiley Online Library or from the author.

Acknowledgements

This work was supported by the European Commission project PHENOMEN (H2020-EU-713450). D.N.U. acknowledges the support of a Ramón y Cajal postdoctoral fellowship (RYC-2014-15392). The authors acknowledge Francesca Bontempi (Scuola Superiore Sant'Anna, Pisa) for ellipsometric measurements, and Francesco Riboli and Sara Nocentini (LENS, Firenze) for optical characterization of a preliminary device.

Conflict of Interest

The authors declare no conflict of interest.

Author Contributions

S.Z. and A.P. conceived the experiment and performed the optical measurements. G.B. provided the epitaxial material and S.Z. fabricated the device. D.M. and L.P. supported the numerical analysis. M.C. contributed to the mechanical characterization. S.Z., A.P., D.N.-U. and A.T. analyzed the results. S.Z. and A.P. wrote the manuscript with suggestions and contributions from all the other authors.

Keywords

chirality, metasurfaces, optomechanics, polarization

Received: September 5, 2019

Revised: October 23, 2019

Published online: December 18, 2019

- [1] M. Aspelmeyer, T. J. Kippenberg, F. Marquardt, *Rev. Mod. Phys.* **2014**, *86*, 1391.
- [2] J. Chan, T. P. M. Alegre, A. H. Safavi-Naeini, J. T. Hill, A. Krause, S. Gröblacher, M. Aspelmeyer, O. Painter, *Nature* **2011**, *478*, 89.
- [3] A. H. Safavi-Naeini, S. Gröblacher, J. T. Hill, J. Chan, M. Aspelmeyer, O. Painter, *Nature* **2013**, *500*, 185.
- [4] T. P. Purdy, P.-L. Yu, R. W. Peterson, N. S. Kampel, C. A. Regal, *Phys. Rev. X* **2013**, *3*, 031012.
- [5] K. Hammerer, C. Genes, D. Vitali, P. Tombesi, G. Milburn, C. Simon, D. Bouwmeester, in *Cavity Optomechanics: Nano- and Micromechanical Resonators Interacting with Light* (Eds: M. Aspelmeyer, T. J. Kippenberg, F. Marquardt), Springer, Berlin, Heidelberg **2014**, pp. 25–56.
- [6] D. Navarro-Urrios, N. E. Capuj, M. F. Colombano, P. D. García, M. Sledzinska, F. Alzina, A. Griol, A. Martínez, C. M. Sotomayor-Torres, *Nat. Commun.* **2017**, *8*, 14965.
- [7] M. Winger, T. D. Blasius, T. P. Mayer Alegre, A. H. Safavi-Naeini, S. Meenehan, J. Cohen, S. Stobbe, O. Painter, *Opt. Express* **2011**, *19*, 24905.
- [8] A. Pitanti, J. M. Fink, A. H. Safavi-Naeini, J. T. Hill, C. U. Lei, A. Tredicucci, O. Painter, *Opt. Express* **2015**, *23*, 3196.
- [9] K. C. Balram, M. I. Davanço, J. D. Song, K. Srinivasan, *Nat. Photonics* **2016**, *10*, 346.
- [10] A. Arbabi, Y. Horie, M. Bagheri, A. Faraon, *Nat. Nanotechnol.* **2015**, *10*, 937.
- [11] S. Jahani, Z. Jacob, *Nat. Nanotechnol.* **2016**, *11*, 23.
- [12] D. Neshev, I. Aharonovich, *Light: Sci. Appl.* **2018**, *7*, 58.
- [13] S. Liu, P. P. Vabishchevich, A. Vaskin, J. L. Reno, G. A. Keeler, M. B. Sinclair, I. Staude, I. Brener, *Nat. Commun.* **2018**, *9*, 2507.
- [14] W. Liu, Z. Li, Z. Li, H. Cheng, C. Tang, J. Li, S. Chen, J. Tian, *Adv. Mater.* **2019**, *31*, 1901729.
- [15] L. Zhang, X. Q. Chen, R. W. Shao, J. Y. Dai, Q. Cheng, G. Castaldi, V. Galdi, T. J. Cui, *Adv. Mater.* **2019**, *31*, 1904069.
- [16] T. Starkey, P. Vukusic, *Nanophotonics* **2013**, *2*, 289.
- [17] A. Y. Zhu, W. T. Chen, A. Zaidi, Y. Huang, M. Khorasaninejad, V. Sanjeev, C. Qiu, F. Capasso, *Light: Sci. Appl.* **2018**, *7*, 17158.
- [18] Q. Wang, E. Plum, Q. Yang, X. Zhang, Q. Xu, Y. Xu, J. Han, W. Zhang, *Light: Sci. Appl.* **2018**, *7*, 25.
- [19] V. S. Asadchy, A. Díaz-Rubio, S. A. Tretyakov, *Nanophotonics* **2018**, *7*, 1069.
- [20] J. T. Collins, C. Kuppe, D. C. Hooper, C. Sibia, M. Centini, V. K. Valev, *Adv. Opt. Mater.* **2017**, *5*, 1700182.
- [21] C. Wu, N. Arju, G. Kelp, J. A. Fan, J. Dominguez, E. Gonzales, E. Tutuc, I. Brener, G. Shvets, *Nat. Commun.* **2014**, *5*, 3892.
- [22] M. Hentschel, M. Schäferling, X. Duan, H. Giessen, N. Liu, *Sci. Adv.* **2017**, *3*, e1602735.
- [23] T. Kan, A. Isozaki, N. Kanda, N. Nemoto, K. Konishi, H. Takahashi, M. Kuwata-Gonokami, K. Matsumoto, I. Shimoyama, *Nat. Commun.* **2015**, *6*, 8422.
- [24] N. Courjal, S. Benchabane, J. Dahdah, G. Ulliac, Y. Gruson, V. Laude, *Appl. Phys. Lett.* **2010**, *96*, 131103.
- [25] M. M. De Lima, P. V. Santos, *Rep. Prog. Phys.* **2005**, *68*, 1639.
- [26] X. Liu, W. J. Padilla, *Adv. Opt. Mater.* **2013**, *1*, 559.
- [27] M. Liu, M. Susli, D. Silva, G. Putrino, H. Kala, S. Fan, M. Cole, L. Faraone, V. P. Wallace, W. J. Padilla, D. A. Powell, I. V. Shadrivov, M. Martyniuk, *Microsyst. Nanoeng.* **2017**, *3*, 17033.
- [28] V. Laude, A. Belkhir, A. F. Alabiad, M. Addouche, S. Benchabane, A. Khelif, F. I. Baida, *Optica* **2017**, *4*, 1245.
- [29] N. I. Zheludev, E. Plum, *Nat. Nanotechnol.* **2016**, *11*, 16.
- [30] J.-Y. Ou, E. Plum, J. Zhang, N. I. Zheludev, *Nat. Nanotechnol.* **2013**, *8*, 252.
- [31] M. Liu, D. A. Powell, R. Guo, I. V. Shadrivov, Y. S. Kivshar, *Adv. Opt. Mater.* **2017**, *5*, 1600760.
- [32] M.-X. Ren, W. Wu, W. Cai, B. Pi, X.-Z. Zhang, J.-J. Xu, *Light: Sci. Appl.* **2017**, *6*, e16254.
- [33] D. Balestri, M. Petruzzella, S. Checcucci, F. Intonti, N. Caselli, F. Sgrignuoli, F. W. M. Otten, A. Fiore, M. Gurioli, *Adv. Mater.* **2019**, *31*, 1807274.
- [34] H. Zhu, F. Yi, E. Cubukcu, *Nat. Photonics* **2016**, *10*, 709.
- [35] M. M. de Lima, R. Hey, P. V. Santos, *Appl. Phys. Lett.* **2003**, *83*, 2997.
- [36] S. A. Campbell, *The Science and Engineering of Microelectronic Fabrication*, Oxford University Press, Oxford **2001**.
- [37] S. V. Lobanov, S. G. Tikhodeev, N. A. Gippius, A. A. Maksimov, E. V. Filatov, I. I. Tartakovskii, V. D. Kulakovskii, T. Weiss, C. Schneider, J. Geßler, M. Kamp, S. Höfling, *Phys. Rev. B* **2015**, *92*, 205309.
- [38] R. Ohta, H. Okamoto, T. Tawara, H. Gotoh, H. Yamaguchi, *Phys. Rev. Lett.* **2018**, *120*, 267401.
- [39] T. Watanabe, H. Okamoto, K. Onomitsu, H. Gotoh, T. Sogawa, H. Yamaguchi, *Appl. Phys. Lett.* **2012**, *101*, 082107.

- [40] R. Camacho-Morales, M. Rahmani, S. Kruk, L. Wang, L. Xu, D. A. Smirnova, A. S. Solntsev, A. Miroschnichenko, H. H. Tan, F. Karouta, S. Naureen, K. Vora, L. Carletti, C. De Angelis, C. Jagadish, Y. S. Kivshar, D. N. Neshev, *Nano Lett.* **2016**, *16*, 7191.
- [41] E. V. Melik-Gaykazyan, S. S. Kruk, R. Camacho-Morales, L. Xu, M. Rahmani, K. Zangeneh Kamali, A. Lamprianidis, A. E. Miroschnichenko, A. A. Fedyanin, D. N. Neshev, Y. S. Kivshar, *ACS Photonics* **2018**, *5*, 728.
- [42] G. Li, S. Zhang, T. Zentgraf, *Nat. Rev. Mater.* **2017**, *2*, 17010.
- [43] L. Carletti, D. Rocco, A. Locatelli, C. De Angelis, V. F. Gili, M. Ravaro, I. Favero, G. Leo, M. Finazzi, L. Ghirardini, M. Celebrano, G. Marino, A. V. Zayats, *Nanotechnology* **2017**, *28*, 114005.
- [44] L. Ding, C. Baker, P. Senellart, A. Lemaitre, S. Ducci, G. Leo, I. Favero, *Phys. Rev. Lett.* **2010**, *105*, 263903.
- [45] A. Chowdhury, S. Barbay, M. G. Clerc, I. Robert-Philip, R. Braive, *Phys. Rev. Lett.* **2017**, *119*, 234101.
- [46] W. Ye, X. Yuan, C. Guo, J. Zhang, B. Yang, S. Zhang, *Phys. Rev. Appl.* **2017**, *7*, 054003.
- [47] C. Menzel, C. Rockstuhl, F. Lederer, *Phys. Rev. A* **2010**, *82*, 053811.
- [48] S. Zannotto, G. Mazzamuto, F. Riboli, G. Biasiol, G. C. La Rocca, A. Tredicucci, A. Pitanti, *Nanophotonics* **2019**, *8*, 2291.
- [49] Y. Tang, A. E. Cohen, *Phys. Rev. Lett.* **2010**, *104*, 163901.
- [50] I. Fernandez-Corbaton, M. Fruhnert, C. Rockstuhl, *Phys. Rev. X* **2016**, *6*, 031013.
- [51] C. Hao, L. Xu, H. Kuang, C. Xu, *Adv. Mater.* **2019**, 1802075, <https://doi.org/10.1002/adma.201802075>.
- [52] D. Woolf, P.-C. Hui, E. Iwase, M. Khan, A. W. Rodriguez, P. Deotare, I. Bulu, S. G. Johnson, F. Capasso, M. Loncar, *Opt. Express* **2013**, *21*, 7258.
- [53] C. Baker, W. Hease, D.-T. Nguyen, A. Andronico, S. Ducci, G. Leo, I. Favero, *Opt. Express* **2014**, *22*, 14072.